PTEP

Prog. Theor. Exp. Phys. **2022** 093D02(14 pages)
DOI: 10.1093/ptep/ptac100

IYBSSD2022
International Year
of Basic Sciences
for Sustainable Development

Anomalous enhancement of dilepton production as a precursor of color superconductivity

Toru Nishimura[1], Masakiyo Kitazawa[1,2], and Teiji Kunihiro[3]

[1] *Department of Physics, Osaka University, Toyonaka, Osaka 560-0043, Japan*
[2] *J-PARC Branch, KEK Theory Center, Institute of Particle and Nuclear Studies, KEK, 319-1106, Japan*
[3] *Yukawa Institute for Theoretical Physics, Kyoto University, Kyoto 606-8502, Japan*
*E-mail: nishimura@kern.phys.sci.osaka-u.ac.jp

Received April 21, 2022; Revised July 11, 2022; Accepted July 26, 2022; Published July 28, 2022

We compute the modification of the photon self-energy due to dynamical diquark fluctuations developed near the critical temperature of two-flavor superconductivity, which is one of the color superconducting phases, through the Aslamasov–Larkin, Maki–Thompson, and density of states terms, which are responsible for the paraconductivity in metals at vanishing energy and momentum. The analysis is performed through an investigation of the diquark fluctuations within the normal phase determined by the mean-field approximation in the massless two-flavor Nambu–Jona-Lasinio model. It is shown that the rate has a significant enhancement in low-invariant-mass regions over a rather wide range of temperatures in the normal phase. This enhancement is worth exploring in the relativistic heavy-ion collisions, which may thereby reveal the significance of the diquark fluctuations in dense quark matter.

Subject Index C00, C50, D30, D31

1. Introduction

Revealing the rich phase structure and thereby developing a condensed matter physics of quantum chromodynamics (QCD) in high-density regions is one of the main subjects in current nuclear physics [1,2], and a great deal of work is being done both theoretically and experimentally. In a high-density region, for instance, first-order chiral transition line(s) with QCD critical point(s) are expected to exist on the basis of theoretical works [3–5], and the experimental search for these phase transitions [6] is one of the main purposes of the beam-energy scan program in the relativistic heavy-ion collisions (HIC) at RHIC, HADES, and NA61/SHINE; further studies to reveal the phase structure with higher statistics will be pursued in future experiments planned at GSI-FAIR, NICA-MPD, and J-PARC-HI [7]. Such studies on the Earth will also provide us with invaluable information on the interior structure of compact stars [8–10].

An interesting feature of the dense quark matter in yet higher-density regions is the possible realization of color superconductivity (CSC) induced by the condensation of diquark Cooper pairs [11]. Now that future HIC experiments are designed so as to enable detailed analyses of

Funded by SCOAP[3]. SCOAP3 and OUP support the goals of the International Year of Basic Sciences for Sustainable Development

dense matter, it would be intriguing to explore the possible existence of the CSC phases in these experiments. The search for CSC in HIC, however, is quite a challenge because the temperatures T achieved in HIC can become as high as 100 MeV at the highest baryon density [12], which may be much higher than the critical temperature T_c of CSC, and hence an observation of the CSC phases may be unlikely in HIC.

Nevertheless, the matter created in HIC may be within the critical region above T_c where the diquark-pair fluctuations are significant, and thus *precursory phenomena* of the CSC [13–15] do manifest themselves through appropriate observables by HIC. In this respect, it is suggestive that fluctuations of Cooper pairs (preformed pairs) of electrons in metals are known to cause an anomalous enhancement of the electric conductivity above T_c of the superconductivity (SC) [16–18]. Moreover, since the quark matter in the relevant density region is a strongly coupled system [14,19], CSC can have a wider critical region where the precursory phenomena of CSC are pronounced. In fact, it has already been shown [13–15,20–23] that the diquark fluctuations develop a well-defined collective mode, which is the soft mode of CSC, and its collectivity and the softening nature affect various observables including the appearance of the "pseudogap" region [14] in a rather wide range of temperature.

In the present article, we investigate possible enhancement of the production rate of virtual photons due to the precursory diquark fluctuations, which is to be observed as the dilepton production rate (DPR) in HIC. A desirable feature of the electromagnetic probes, needless to say, lies in the fact that the interactions of the probes with the medium are weak, and their properties are hardly modified from what they had when created, in contrast to hadronic signals.

Here we remark that the DPR *within* the CSC phases *below* T_c is known to show some unique behavior [24]. It is also possible that collective excitations in the CSC phases affect the DPR. However, such behaviors becomes weaker when T goes higher and closer to T_c because they are caused by the finite diquark gap. On the other hand, the precursory phenomena to be investigated in the present paper are most enhanced at $T = T_c$, which is an attractive feature in HIC.

The medium modification of the DPR or the virtual photons is dictated by that of the photon self-energy [25–27]. The effects of the diquark fluctuations on the photon self-energy can be taken into account by the Aslamasov–Larkin (AL), Maki–Thompson (MT), and density of states (DOS) terms [15,21,23]. In the case of metallic SC, these terms at the vanishing energy–momentum limit are known to explain the anomalous enhancement of the electric conductivity above T_c [16,18].

In the present article, we calculate AL, MT, and DOS terms composed of diquark fluctuations near but above T_c of the two-flavor superconductor (2SC), which is one of the CSC phases that is believed to be realized at relatively low density with a realistic strange quark mass [11]. We show that the Ward–Takahashi (WT) identity is satisfied by summing up all of these terms. From the imaginary part of these terms we calculate a virtual photon emission from the diquark fluctuations that form a collective mode. Although a single diquark excitation is not gauge invariant, the photon self-energy and hence the DPR can be affected by the diquark fluctuations in a gauge invariant way through these terms. It is found that the virtual photons emitted from the collective modes with spectral support in the space-like region in turn have spectral support in the time-like region. Our numerical results show that the DPR is significantly enhanced in the low-invariant-mass region $M \lesssim 200$ MeV above T_c up to, say, $T \simeq 1.5T_c$, reflecting the critical enhancement of the diquark fluctuations. We argue that experimental measurement of

dileptons and exploration of the possible enhancement of the DPR in that very low-mass region in HIC are quite worthwhile because they would give experimental evidence of strong diquark correlations as a precursor to the phase transition to 2SC in dense quark matter.

2. Model and phase diagram

Among various CSC phases, the phase with the highest probability of being realized in the medium within the reach of HIC is 2SC [11]. In the present study, we thus focus on the diquark fluctuations around the phase boundary of this phase above T_c. To describe the phase transition to 2SC we employ the two-flavor Nambu–Jona-Lasinio (NJL) model [28,29] as an effective model of QCD:

$$\mathcal{L} = \bar{\psi} i\partial\!\!\!/ \psi + \mathcal{L}_{\rm S} + \mathcal{L}_{\rm C}, \tag{1}$$

$$\mathcal{L}_{\rm S} = G_{\rm S}[(\bar{\psi}\psi)^2 + (\bar{\psi} i\gamma_5 \vec{\tau}\psi)^2], \tag{2}$$

$$\mathcal{L}_{\rm C} = G_{\rm C}(\bar{\psi} i\gamma_5 \tau_2 \lambda_A \psi^C)(\bar{\psi}^C i\gamma_5 \tau_2 \lambda_A \psi), \tag{3}$$

where $\mathcal{L}_{\rm S}$ and $\mathcal{L}_{\rm C}$ represent the quark–antiquark and quark–quark interactions, respectively, and $\psi^C(x) = i\gamma_2\gamma_0\bar{\psi}^T(x)$. τ_2 and λ_A ($A = 2, 5, 7$) are the antisymmetric components of the Pauli and Gell-Mann matrices for the flavor $SU(2)_f$ and color $SU(3)_c$, respectively. The scalar coupling constant $G_{\rm S} = 5.01\,{\rm GeV}^{-2}$ and the three-momentum cutoff $\Lambda = 650$ MeV are determined so as to reproduce the pion decay constant $f_\pi = 93$ MeV and the chiral condensate $\langle\bar{\psi}\psi\rangle = (-250\,{\rm MeV})^3$ in vacuum [28]. Since explicit chiral symmetry breaking plays just a minor role and is virtually irrelevant in the diquark fluctuations around the critical temperature [15], we neglect the current quark mass for simplicity. The magnitude of the diquark coupling $G_{\rm C}$ has been discussed in the literature based on the Fierz transformation of the one-gluon exchange interaction, the instanton-induced interaction, the diquark–quark picture of baryons, renormalization group analysis, etc.; see, e.g., Ref. [29] and references therein. In the present study we treat $G_{\rm C}$ as a free parameter and vary it within the interval $G_{\rm C}/G_{\rm S} = 0.5$–$0.9$, which is an intermediate range among these studies. We employ a common quark chemical potential μ for up and down quarks since the effect of isospin breaking is not large in the medium created in HIC.

In Fig. 1, we show the phase diagram in the T–μ plane obtained in the mean-field approximation (MFA) with the mean fields $\langle\bar{\psi}\psi\rangle$ and $\langle\bar{\psi}^C\Gamma\psi\rangle$ with $\Gamma = i\gamma_5\tau_2\lambda_A$. The bold lines show the phase diagram at $G_{\rm C} = 0.7G_{\rm S}$, where the solid and dashed lines represent the first- and second-order phase transitions, respectively. The 2SC phase is realized in the dense region at relatively low temperatures. In the figure, the phase boundary of 2SC for $G_{\rm C} = 0.5G_{\rm S}$ and $0.9G_{\rm S}$ is also shown by the thin dotted lines.

In MFA, the phase transition to 2SC is of second order, as seen in Fig. 1. It should be mentioned here that the transition may become first order when the fluctuation effect of gauge fields (gluons) is incoporated in asymptotically high-density regions [30–32], which might persist at lower densities [33]. We also remark that the nature of the phase transition might be modified even within the NJL model when effects beyond the MFA are incorporated, although such an analysis has never been performed in the literature to the best of the authors' knowledge. In any event, it is not yet settled whether the phase transition to a 2SC phase at low densities is

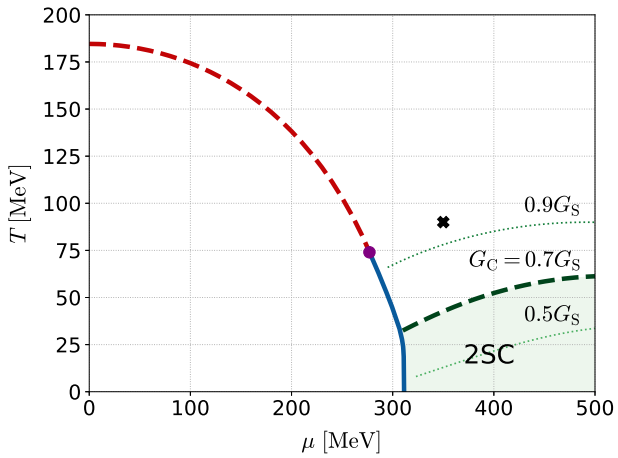

Fig. 1. Phase diagram obtained in the massless two-flavor NJL model (1). The bold lines show the transition lines at $G_C = 0.7G_S$. The solid and dashed lines represent the first- and second-order phase transitions. T_c values of the 2SC phase at $G_C = 0.5G_S$ and $0.9G_S$ are also shown by the thin dotted lines.

Fig. 2. Diagrammatic representation of the T-matrix (6) in the RPA.

of second or first order, including its strength. In the present study, we thus assume that the transition is of second or weak first order with the formation of the soft mode discussed below.

3. The soft mode of 2SC

3.1 *Propagator of the diquark field*

A characteristic feature of the second-order phase transition is that the fluctuation amplitude of the order parameter diverges at $T = T_c$. To see such a divergence at the T_c value of 2SC, let us consider the imaginary-time propagator of the colored diquark field $\Delta(x) = \bar{\psi}^C(x)\Gamma\psi(x)$,

$$\mathcal{D}(k) = -\int_0^{1/T} d\tau \int d^3\boldsymbol{x} \langle T_\tau \Delta^\dagger(x)\Delta(0)\rangle e^{i\nu_l\tau} e^{-i\boldsymbol{k}\cdot\boldsymbol{x}}, \tag{4}$$

where $k = (\boldsymbol{k}, i\nu_l)$ is the four-momentum of the diquark field, with ν_l the Matsubara frequency for bosons, τ is the imaginary time, and T_τ denotes the imaginary-time ordering. In the random-phase approximation (RPA), Eq. (4) is given by $\mathcal{D}(k) = \mathcal{Q}(k)/(1 + G_C\mathcal{Q}(k))$ with the one-loop quark–quark correlation function

$$\mathcal{Q}(k) = -8\int_p \mathrm{Tr}[\mathcal{G}_0(k-p)\mathcal{G}_0(p)], \tag{5}$$

where $\mathcal{G}_0(p) = 1/[(i\omega_m + \mu)\gamma_0 - \boldsymbol{p}\cdot\boldsymbol{\gamma}]$ is the free-quark propagator with $p = (\boldsymbol{p}, i\omega_m)$ and the Matsubara frequency for fermions ω_m, Tr denotes the trace over the Dirac indices, and $\int_p = T\sum_m \int d^3\boldsymbol{p}/(2\pi)^3$. We also introduce the T-matrix to describe the diquark fluctuation

$$\tilde{\Xi}(k) = \frac{1}{G_C^{-1} + \mathcal{Q}(k)} = G_C - G_C\mathcal{D}(k)G_C, \tag{6}$$

which is diagrammatically represented in Fig. 2.

The retarded Green's functions $D^R(\boldsymbol{k}, \omega)$, $Q^R(\boldsymbol{k}, \omega)$, and $\Xi^R(\boldsymbol{k}, \omega)$ corresponding to Eqs. (4)–(6), respectively, are obtained by the analytic continuation $i\nu_l \to \omega + i\eta$. The imaginary part of

$Q^R(\boldsymbol{k}, \omega)$ is calculated to be [15]

$$\mathrm{Im}Q^R(\boldsymbol{k}, \omega) = -\frac{2T}{\pi k}[(\omega + 2\mu)^2 - k^2]\left\{ \log \frac{\cosh(\omega + k)/4T}{\cosh(\omega - k)/4T} - \frac{\omega}{2T}\theta(k - |\omega + 2\mu|)\right\}. \quad (7)$$

Its real part is then constructed using the Kramers–Kronig relation

$$\mathrm{Re}Q^R(\boldsymbol{k}, \omega) = \frac{1}{\pi} P \int_{-2\Lambda-2\mu}^{2\Lambda-2\mu} d\omega' \frac{\mathrm{Im}Q^R(\boldsymbol{k}, \omega)}{\omega' - \omega}\ , \quad (8)$$

where P denotes the principal value [15].

The retarded diquark propagator $D^R(\boldsymbol{k}, \omega)$, and hence the T-matrix $\Xi^R(\boldsymbol{k}, \omega)$, has a pole at $\omega = |\boldsymbol{k}| = 0$ at $T = T_c$; $[D^R(\boldsymbol{0}, 0)]^{-1}_{T=T_c} = [\Xi^R(\boldsymbol{0}, 0)]^{-1}_{T=T_c} = 0$. This fact, known as the Thouless criterion [34], is confirmed by comparing the denominator of $D^R(\boldsymbol{k}, \omega)$ with the gap equation for the diquark field. The criterion shows that the diquark field has a massless collective mode at $T = T_c$. Furthermore, the pole of this collective mode moves continuously toward the origin in the complex energy plane as T is lowered to T_c, and hence the collective mode has a vanishing excitation energy toward T_c. This collective mode is called the *soft mode*. Because of the small excitation energy, they tend to be easily excited and affect various observables in the medium near T_c [14,15].

Although we had recourse to the MFA and RPA, the appearance of a soft mode is a generic feature of the second-order phase transition [17,18], and even if the phase transition is of first order, the development of a collective mode with the softening nature prior to the critical point is still expected for weak first-order transitions. It may be worthwhile to clarify here the difference between the soft mode [17,18] and the Nambu–Goldstone (NG) mode. The latter is a massless mode corresponding to the phase fluctuations of the order parameter with a nonzero expectation value in the broken phase. On the other hand, the soft mode corresponds to the amplitude fluctuations of the order parameter around the zero value in the normal phase, and is not massless except at the critical point. Although the NG mode in the 2SC phase is absorbed into the gauge field and thereby makes the massive longitudinal mode by the Higgs mechanism [11], the soft mode becomes massless at $T = T_c$ even in this case if the phase transition is of second order. Therefore, the emergence of the soft mode in the diquark channel and the following discussions on its effects on observables should have a model-independent validity, at least qualitatively.

We also emphasize that the Thouless criterion implies the appearance of such soft modes even around the phase boundary above T_c of other CSC phases, such as the color–flavor-locked (CFL) phase, provided that the phase transition is of second order. Therefore, the present analysis performed on the 2SC phase can be applied to the diquark soft modes in other CSC phases with a due straightforward modification, although they would be irrelevant to HIC.

To detail the properties of the soft mode, it is convenient to introduce the dynamical structure factor $S(\boldsymbol{k}, \omega)$ given by

$$S(\boldsymbol{k}, \omega) = -\frac{1}{\pi}\frac{1}{1 - e^{-\omega/T}}\mathrm{Im}D^R(\boldsymbol{k}, \omega). \quad (9)$$

Figure 3 shows a contour map of $S(\boldsymbol{k}, \omega)$ at $T = 1.05T_c$ for $\mu = 350$ MeV and $G_{\mathrm{C}} = 0.7G_{\mathrm{S}}$. One sees that $S(\boldsymbol{k}, \omega)$ has a clear spectral concentration with a peak around the origin in the ω–$|\boldsymbol{k}|$ plane, which implies a development of the collective mode having a definite dispersion relation $\omega = \omega(|\boldsymbol{k}|)$ with a small width [13,15]. We also note that the spectral concentration is

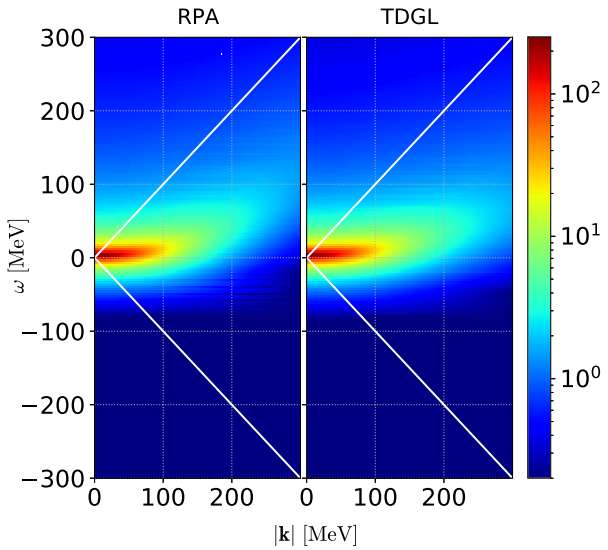

Fig. 3. Contour plot of the dynamical structure factor $S(\boldsymbol{k}, \omega)$ at $T = 1.05T_c$ for $\mu = 350$ MeV and $G_{\rm C} = 0.7G_{\rm S}$. The solid lines show the light cone. The left panel is the result of the RPA obtained from Eqs. (7) and (8), while the right panel is the result in the TDGL approximation (10).

confined in the space-like region, $\omega(|\boldsymbol{k}|) < |\boldsymbol{k}|$. The property will be picked up again later when we discuss the DPR that has a spectral support in the time-like region.

It is to be noted that the properties of the soft mode discussed here persist even with the finite current quark mass, because the structure and properties of particle–particle excitations near the Fermi surface are less affected by the quark mass. This feature is contrasted with mesonic excitations, whose properties around the origin are known to change drastically because their structure around the light cone is strongly modified by the quark mass. On the other hand, the light cone in the diquark propagator $D^R(\boldsymbol{k}, \omega)$ exists at $|\omega + 2\mu| = |\boldsymbol{k}|$ and the origin $(\boldsymbol{k}, \omega) = (0, 0)$ is deep inside the time-like region.

3.2 *Time-dependent Ginzburg–Landau (TDGL) approximation*

Since the diquark fluctuations near T_c have spectral concentration in the low-energy region as we have seen above, we approximate the T-matrix $\Xi^R(\boldsymbol{k}, \omega)$ in the small ω region as

$$\Xi^R(\boldsymbol{k}, \omega) \simeq \frac{1}{c\omega + G_{\rm C}^{-1} + Q^R(\boldsymbol{k}, 0)} , \tag{10}$$

with $c = \partial Q^R(\boldsymbol{0}, \omega)/\partial\omega|_{\omega=0}$. We refer to Eq. (10) as the time-dependent Ginzburg–Landau (TDGL) approximation, since Eq. (10) corresponds to the linearlized TDGL approximation for the T-matrix [35] without the expansion along $|\boldsymbol{k}|^2$. In this study we do not expand $[\Xi^R(\boldsymbol{k}, \omega)]^{-1}$ with respect to $|\boldsymbol{k}|^2$ for a better description of the spectral strength extending along the $|\boldsymbol{k}|$ direction widely as in Fig. 3. An explicit calculation shows that c is a complex number, while $G_{\rm C}^{-1} + Q^R(\boldsymbol{k}, 0)$ is real.

In the right panel of Fig. 3, we show $S(\boldsymbol{k}, \omega)$ obtained by the TDGL approximation. By comparing the result with the left panel, one sees that the TDGL approximation (10) reproduces the result obtained by the RPA quite well in a wide range in the ω–$|\boldsymbol{k}|$ plane.

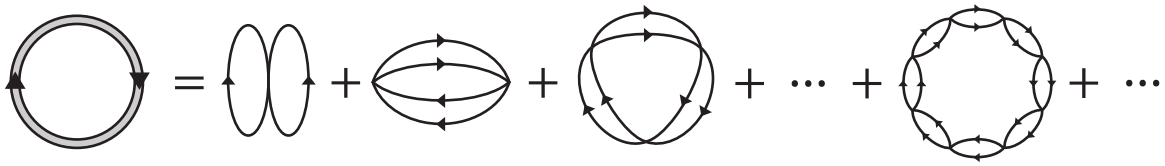

Fig. 4. Contribution of the diquark fluctuations to the thermodynamic potential.

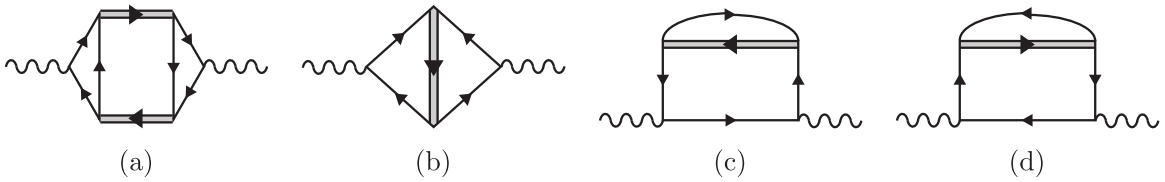

Fig. 5. Diagrammatic representations of the Aslamasov–Larkin (a), Maki–Thompson (b), and density of states (c, d) terms in Eqs. (12)–(14). The double and wavy lines represent diquarks and photons, respectively.

4. Photon self-energy and dilepton production rate

The DPR is given in terms of the retarded photon self-energy $\Pi^{R\mu\nu}(\boldsymbol{k}, \omega)$ as [25–27]

$$\frac{d^4\Gamma(\boldsymbol{k}, \omega)}{d^4k} = -\frac{\alpha}{12\pi^4}\frac{1}{\omega^2 - |\boldsymbol{k}|^2}\frac{1}{e^{\omega/T} - 1} g_{\mu\nu}\mathrm{Im}\Pi^{R\mu\nu}(\boldsymbol{k}, \omega), \tag{11}$$

with the fine structure constant α and the Minkowski metric $g_{\mu\nu}$.

4.1 *Construction of the photon self-energy*

We are now in a position to discuss the way in which the effects of the diquark fluctuations are included in $\Pi^{R\mu\nu}(\boldsymbol{k}, \omega)$. For this, we start from the one-loop diagram of the diquark propagator shown in Fig. 4, which is the lowest-order contribution of the diquark fluctuations to the thermodynamic potential. The photon self-energy is then constructed by attaching electromagnetic vertices at two points of quark lines in Fig. 4. This construction guarantees the WT identity $k_\nu \Pi^{R\mu\nu}(\boldsymbol{k}, \omega) = 0$. This procedure leads to the four types of diagrams shown in Fig. 5, which are called (a) Aslamasov–Larkin (AL) [36], (b) Maki–Thompson (MT) [37,38], and (c, d) density of states (DOS) terms, respectively, in the theory of metallic SC [18]. The respective contributions to the photon self-energy are denoted by $\tilde{\Pi}^{\mu\nu}_{\mathrm{AL}}(k)$, $\tilde{\Pi}^{\mu\nu}_{\mathrm{MT}}(k)$, and $\tilde{\Pi}^{\mu\nu}_{\mathrm{DOS}}(k)$ in the imaginary-time formalism, and are expressed as

$$\tilde{\Pi}^{\mu\nu}_{\mathrm{AL}}(k) = 3\int_q \tilde{\Gamma}^{\mu}(q, q+k)\tilde{\Xi}(q+k)\tilde{\Gamma}^{\nu}(q+k, q)\tilde{\Xi}(q), \tag{12}$$

$$\tilde{\Pi}^{\mu\nu}_{\mathrm{MT}}(k) = 3\int_q \tilde{\Xi}(q)\,\mathcal{R}^{\mu\nu}_{\mathrm{MT}}(q, k), \tag{13}$$

$$\tilde{\Pi}^{\mu\nu}_{\mathrm{DOS}}(k) = 3\int_q \tilde{\Xi}(q)\,\mathcal{R}^{\mu\nu}_{\mathrm{DOS}}(q, k), \tag{14}$$

respectively, where $q = (\boldsymbol{q}, i\nu_n)$ is the four-momentum of a diquark field and the overall coefficients 3 come from three antisymmetric channels of the diquark field. The vertex functions $\tilde{\Gamma}^{\mu}(q, k)$, $\mathcal{R}^{\mu\nu}_{\mathrm{MT}}(q, k)$, and $\mathcal{R}^{\mu\nu}_{\mathrm{DOS}}(q, k)$ in Eqs. (12)–(14) are given by

$$\tilde{\Gamma}^{\mu}(q, q+k) = 8(e_u + e_d)\int_p \mathrm{Tr}[\mathcal{G}_0(p)\gamma^{\mu}\mathcal{G}_0(p+k)\mathcal{G}_0(q-p)], \tag{15}$$

$$\mathcal{R}^{\mu\nu}_{\mathrm{MT}}(q, k) = 16e_u e_d\int_p \mathrm{Tr}[\mathcal{G}_0(p)\gamma^{\mu}\mathcal{G}_0(p+k)\mathcal{G}_0(q-p-k)\gamma^{\nu}\mathcal{G}_0(q-p)], \tag{16}$$

$$\mathcal{R}^{\mu\nu}_{\rm DOS}(q,k) = 8(e_u^2+e_d^2)\int_p \Big\{ {\rm Tr}[\mathcal{G}_0(p)\gamma^\mu \mathcal{G}_0(p+k)\gamma^\nu \mathcal{G}_0(p)\mathcal{G}_0(q-p)] + {\rm Tr}[\mathcal{G}_0(p)\gamma^\mu \mathcal{G}_0(p-k)\gamma^\nu \mathcal{G}_0(p)\mathcal{G}_0(q-p)]\Big\}, \tag{17}$$

where $e_u = 2|e|/3$ and $e_d = -|e|/3$ are the electric charges of up and down quarks, respectively, with the elementary charge e.

The total photon self-energy in imaginary time is given by

$$\tilde{\Pi}^{\mu\nu}(k) = \tilde{\Pi}^{\mu\nu}_{\rm free}(k) + \tilde{\Pi}^{\mu\nu}_{\rm fluc}(k), \tag{18}$$

$$\tilde{\Pi}^{\mu\nu}_{\rm fluc}(k) = \tilde{\Pi}^{\mu\nu}_{\rm AL}(k) + \tilde{\Pi}^{\mu\nu}_{\rm MT}(k) + \tilde{\Pi}^{\mu\nu}_{\rm DOS}(k), \tag{19}$$

where $\tilde{\Pi}^{\mu\nu}_{\rm fluc}(k)$ denotes the modification of the self-energy due to the diquark fluctuations and $\tilde{\Pi}^{\mu\nu}_{\rm free}(k)$ is that of the free-quark system [39,40].

4.2 *Vertices*

The vertices (15)–(17) satisfy the WT identities

$$k_\mu \tilde{\Gamma}^\mu(q,q+k) = e_\Delta\big(\mathcal{Q}(q+k)-\mathcal{Q}(q)\big) = e_\Delta\left(\frac{1}{\tilde{\Xi}(q+k)} - \frac{1}{\tilde{\Xi}(q)}\right), \tag{20}$$

$$k_\mu \mathcal{R}^{\mu\nu}(q,k) = e_\Delta\big(\Gamma^\nu(q-k,q) - \Gamma^\nu(q,q+k)\big), \tag{21}$$

with $\mathcal{R}^{\mu\nu}(q,k) = \mathcal{R}^{\mu\nu}_{\rm MT}(q,k) + \mathcal{R}^{\mu\nu}_{\rm DOS}(q,k)$ and $e_\Delta = e_u + e_d$ being the electric charge of diquarks. Using Eqs. (20), (21) and $\tilde{\Gamma}^\nu(q,q+k) = \tilde{\Gamma}^\nu(q+k,q)$, the WT identity of the photon self-energy $k_\nu \tilde{\Pi}^{\mu\nu}_{\rm fluc}(k) = 0$ is shown explicitly as

$$\begin{aligned} k_\mu \tilde{\Pi}^{\mu\nu}_{\rm fluc}(k) &= k_\mu \tilde{\Pi}^{\mu\nu}_{\rm AL}(k) + k_\mu\big\{\tilde{\Pi}^{\mu\nu}_{\rm MT}(k) + \tilde{\Pi}^{\mu\nu}_{\rm DOS}(k)\big\} \\ &= -3e_\Delta \int_q + 3e_\Delta \int_q \tilde{\Xi}(q)\big[\tilde{\Gamma}^\nu(q-k,q) - \tilde{\Gamma}^\nu(q,q+k)\big] = 0. \end{aligned} \tag{22}$$

Since we adopt the TDGL approximation for $\Xi^R(\boldsymbol{k},\omega)$, the vertices $\tilde{\Gamma}^\mu(q,q+k)$ and $\mathcal{R}^{\mu\nu}(q,k)$ have to be approximated to satisfy Eqs. (20) and (21) within this approximation. From Eq. (10) one finds

$$\begin{aligned} [\tilde{\Xi}(q+k)]^{-1} - [\tilde{\Xi}(q)]^{-1} &\simeq c_0 i\nu_n + \mathcal{Q}(\boldsymbol{q}+\boldsymbol{k},0) - \mathcal{Q}(\boldsymbol{q},0) \\ &= c_0 i\nu_n + \frac{\mathcal{Q}(\boldsymbol{q}+\boldsymbol{k},0)-\mathcal{Q}(\boldsymbol{q},0)}{|\boldsymbol{q}+\boldsymbol{k}|^2-|\boldsymbol{q}|^2}(|\boldsymbol{q}+\boldsymbol{k}|^2-|\boldsymbol{q}|^2) \\ &= c_0 i\nu_n + \mathcal{Q}_{(1)}(\boldsymbol{q}+\boldsymbol{k},\boldsymbol{q})\,(2\boldsymbol{q}+\boldsymbol{k})\cdot\boldsymbol{k}, \end{aligned} \tag{23}$$

where $\mathcal{Q}_{(1)}(\boldsymbol{q}_1,\boldsymbol{q}_2) = (\mathcal{Q}(\boldsymbol{q}_1,0)-\mathcal{Q}(\boldsymbol{q}_2,0))/(|\boldsymbol{q}_1|^2-|\boldsymbol{q}_2|^2)$ is finite in the limit $|\boldsymbol{q}_1-\boldsymbol{q}_2|\to 0$ because $\mathcal{Q}(\boldsymbol{q},\omega)$ is a function of $|\boldsymbol{q}|^2$. Substituting Eq. (23) into Eq. (20) and requiring the analyticity of $\tilde{\Gamma}^\mu(q,q+k)$ at $\omega = |\boldsymbol{k}| = 0$, one finds that $\tilde{\Gamma}^0(q,q+k) = e_\Delta c_0$ and

$$\tilde{\Gamma}^i(q,q+k) = -e_\Delta \mathcal{Q}_{(1)}(\boldsymbol{q}+\boldsymbol{k},\boldsymbol{q})(2q+k)^i \tag{24}$$

are choices that satisfy Eq. (20), where $i = 1, 2, 3$. One can also obtain forms of $\mathcal{R}^{\mu\nu}(q,k)$ satisfying Eq. (21) with Eq. (24) in a similar manner; these, however, are not shown explicitly since they turn out to be unnecessary in this study, as discussed below. These vertices with Eq. (10) satisfy the WT identity of $\tilde{\Pi}^{\mu\nu}(k)$. The reader should be warned, however, that the uniqueness of the choice of Eq. (24) holds only in the lowest order of ω and $|\boldsymbol{k}|^2$, and hence the non-uniqueness may affect the final result in the high-energy region.

4.3 *Dilepton production rate*

In the above construction of $\tilde{\Gamma}^{\mu}(q, q+k)$ and $\mathcal{R}^{\mu\nu}(q,k)$, the spatial components of these vertices are real. This fact greatly simplifies the analytic continuation from $\tilde{\Pi}^{ij}_{\rm fluc}(k)$ to $\Pi^{Rij}_{\rm fluc}(\boldsymbol{k},\omega)$. From the reality of $\mathcal{R}^{ij}(q,k)$ it is also shown that $\mathrm{Im}[\Pi^{Rij}_{\rm MT}(\boldsymbol{k},\omega)+\Pi^{Rij}_{\rm DOS}(\boldsymbol{k},\omega)]=0$ [18], which means that the spatial components $\mathrm{Im}\Pi^{Rij}_{\rm fluc}(\boldsymbol{k},\omega)$ only come from $\Pi^{Rij}_{\rm AL}(\boldsymbol{k},\omega)$, while the temporal component $\mathrm{Im}\Pi^{R00}_{\rm fluc}(\boldsymbol{k},\omega)$ is given by the sum of the AL, MT, and DOS terms. The temporal component, however, is obtained from the spatial ones using the WT identity

$$\tilde{\Pi}^{00}(k)=\frac{\boldsymbol{k}^2}{(i\nu_l)^2}\tilde{\Pi}^{11}(k), \tag{25}$$

with $k=(i\nu_l,|\boldsymbol{k}|,0,0)$. One then finds that $g_{\mu\nu}\tilde{\Pi}^{\mu\nu}_{\rm fluc}(k)$ in Eq. (11) is obtained only from $\Pi^{Rij}_{\rm AL}(\boldsymbol{k},\omega)$ as

$$\begin{aligned}
g_{\mu\nu}\tilde{\Pi}^{\mu\nu}_{\rm fluc}(k)&=\frac{\boldsymbol{k}^2}{(i\nu_l)^2}\tilde{\Pi}^{11}_{\rm AL}(k)-\sum_{i=1}^{3}\tilde{\Pi}^{ii}_{\rm AL}(k)\\
&=3\int\frac{d^3\boldsymbol{q}}{(2\pi)^3}\left[\frac{\boldsymbol{k}^2}{(i\nu_l)^2}\big(\tilde{\Gamma}^1(q,q+k)\big)^2-\sum_i\big(\tilde{\Gamma}^i(q,q+k)\big)^2\right]\\
&\quad\times\oint_C\frac{dq_0}{2\pi i}\frac{\coth\frac{q_0}{2T}}{2}\tilde{\Xi}(\boldsymbol{q}+\boldsymbol{k},q_0+i\nu_l)\tilde{\Xi}(\boldsymbol{q},q_0) \qquad (26)\\
&=3\int\frac{d^3\boldsymbol{q}}{(2\pi)^3}\left[\frac{\boldsymbol{k}^2}{(i\nu_l)^2}\big(\tilde{\Gamma}^1(q,q+k)\big)^2-\sum_i\big(\tilde{\Gamma}^i(q,q+k)\big)^2\right]\\
&\quad\times\left\{P\int\frac{d\omega'}{2\pi i}\frac{\coth\frac{\omega'}{2T}}{2}\Xi^R(\boldsymbol{q}+\boldsymbol{k},\omega'+i\nu_l)\Xi^R(\boldsymbol{q},\omega')\right.\\
&\quad-P\int\frac{d\omega'}{2\pi i}\frac{\coth\frac{\omega'}{2T}}{2}\Xi^R(\boldsymbol{q}+\boldsymbol{k},\omega'+i\nu_l)\Xi^A(\boldsymbol{q},\omega')\\
&\quad+P\int\frac{d\omega'}{2\pi i}\frac{\coth\frac{\omega'}{2T}}{2}\Xi^R(\boldsymbol{q}+\boldsymbol{k},\omega')\Xi^A(\boldsymbol{q},\omega'-i\nu_l)\\
&\quad\left.-P\int\frac{d\omega'}{2\pi i}\frac{\coth\frac{\omega'}{2T}}{2}\Xi^A(\boldsymbol{q}+\boldsymbol{k},\omega')\Xi^A(\boldsymbol{q},\omega'-i\nu_l)\right\}, \qquad (27)
\end{aligned}$$

where the contour C in Eq. (26) surrounds the poles of $\coth(q_0/2T)$ and $\Xi^A(\boldsymbol{k},\omega)=\tilde{\Xi}(k)|_{i\nu_l\to\omega-i\eta}$ is the advanced T-matrix. The far right-hand side of Eq. (27) is obtained after deforming the contour C avoiding the cut in $\tilde{\Xi}(q)$ on the real axis [18]. By taking the analytic continuation $i\nu_l\to\omega+i\eta$ and using $\Xi^A(\boldsymbol{k},\omega)=[\Xi^R(\boldsymbol{k},\omega)]^*$, we obtain

$$\begin{aligned}
g_{\mu\nu}\mathrm{Im}\Pi^{R\mu\nu}_{\rm fluc}(\boldsymbol{k},\omega)&=3e_\Delta^2\int_{-2\Lambda-2\mu}^{2\Lambda-2\mu}\frac{d\omega'}{2\pi}\int\frac{d^3\boldsymbol{q}}{(2\pi)^3}\coth\frac{\omega'}{2T}\\
&\quad\times\big(Q_{(1)}(\boldsymbol{q}+\boldsymbol{k},\boldsymbol{q})\big)^2\left[\left(\frac{(\boldsymbol{q}+\boldsymbol{k})^2-\boldsymbol{q}^2}{\omega}\right)^2-(2\boldsymbol{q}+\boldsymbol{k})^2\right]\\
&\quad\times\mathrm{Im}\Xi^R(\boldsymbol{q}+\boldsymbol{k},\omega')\Big\{\mathrm{Im}\Xi^R(\boldsymbol{q},\omega'+\omega)-\mathrm{Im}\Xi^R(\boldsymbol{q},\omega'-\omega)\Big\}. \qquad (28)
\end{aligned}$$

To deal with the momentum integral in Eq. (28), we introduce the ultraviolet cutoff with the same procedure as in Ref. [15]. The DPR is obtained by substituting this result into Eq. (11).

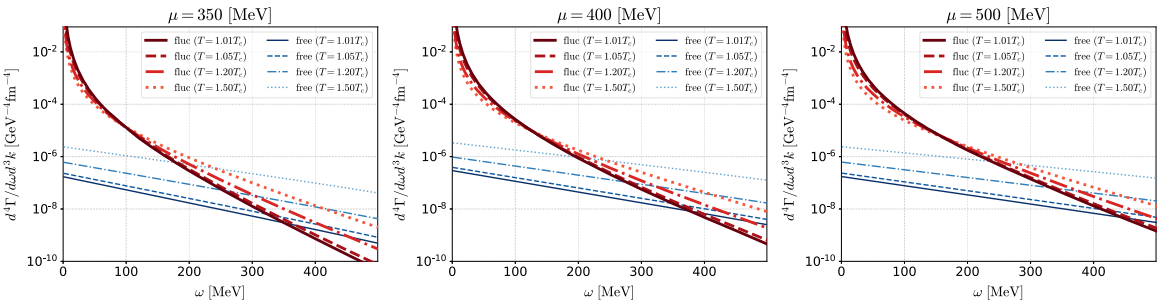

Fig. 6. Dilepton production rates per unit energy and momentum $d^4\Gamma/d\omega d^3k$ at $\boldsymbol{k} = 0$ for several values of T/T_c with $\mu = 350$ MeV (left), 400 MeV (middle), and 500 MeV (right) and $G_{\rm C} = 0.7G_{\rm S}$. The thick red (thin blue) lines show the contribution of $\tilde{\Pi}^{\mu\nu}_{\rm fluc}(k)$ ($\tilde{\Pi}^{\mu\nu}_{\rm free}(k)$).

Before closing this section, we make several remarks on the AL, MT, and DOS terms. First, it is noteworthy that the fluctuations of the *colored* diquark field are coupled to *colorless* photon field through these terms. This nontrivial complication due to the color degrees of freedom is absent in and contrasted with these terms for metallic superconductors. Second, it is possible to consider the modification of $\tilde{\Pi}^{\mu\nu}_{\rm fluc}(k)$ through the AL, MT, and DOS terms but the diquark propagators are replaced with those of the mesonic modes. These terms will affect $\tilde{\Pi}^{\mu\nu}_{\rm fluc}(k)$ significantly when the softening of the mesonic modes takes place. Since such a softening in the mesonic channel occurs at the QCD critical point, this effect should have a non-negligible contribution there. We will come back to this point in Sect. 6.

5. Numerical results

In Fig. 6, we show the numerical results of the production rate $d^4\Gamma/d^4k$ per unit energy and momentum at $\boldsymbol{k} = \boldsymbol{0}$ calculated with use of the photon self-energy (18), (28) for various values of T and μ at $G_{\rm C} = 0.7G_{\rm S}$. The thick lines show the contribution of diquark fluctuations obtained from $\Pi^{R\mu\nu}_{\rm fluc}(\boldsymbol{k}, \omega)$, while the thin lines are the results for the free-quark gas. The total rate is given by the sum of these two contributions. The figure shows that the production rate is enhanced so much by the diquark fluctuations that it greatly exceeds that of the free quarks in the low-energy region $\omega \lesssim 300$ MeV. The enhancement is more pronounced as T is lowered toward T_c, while the enhancement at $\omega \simeq 200$ MeV is observed up to $T \simeq 1.5T_c$. The figure also shows that the contribution of diquark fluctuations is more enhanced as μ becomes larger. This behavior is understood as the effect of the larger Fermi surface for larger μ.

It is worth scrutinizing the underlying mechanism of the low-energy enhancement of the production mechanism of virtual photons. Although it is rather natural that $d^4\Gamma/d^4k$ is enhanced in the low-energy region since the virtual photons are emitted from the soft collective modes, their pronounced effects on the production of virtual photons in the *time-like* region deserves elucidation since the soft mode has a dominant strength in the *space-like* region as shown in Fig. 3. In our formalism, the virtual photons are dominantly emitted through the process obtained by cutting Fig. 5(a), i.e., the scattering of diquarks shown in the left panel of Fig. 7. In this process, the energy–momentum of the virtual photon $k = (\boldsymbol{k}, \omega)$ can be time-like, $\omega > |\boldsymbol{k}|$, since the absolute value of the momentum $\boldsymbol{k} = \boldsymbol{q}_1 - \boldsymbol{q}_2$ can be taken arbitrarily small keeping $\omega = \omega_1 - \omega_2$ finite. This kinematics is contrasted with the scattering of massless quarks shown in the right panel of Fig. 7, in which the produced virtual photon is always in the space-like region $\omega < |\boldsymbol{k}|$. However, $\omega = \omega_1 - \omega_2$ of a virtual photon is restricted to small values due to

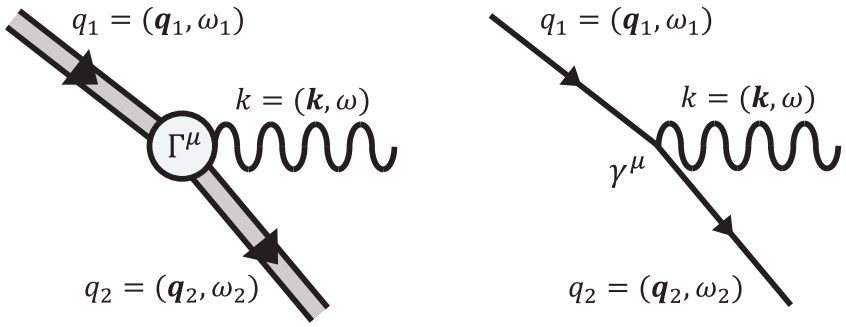

Fig. 7. Diagrams representing the processes of virtual photon production.

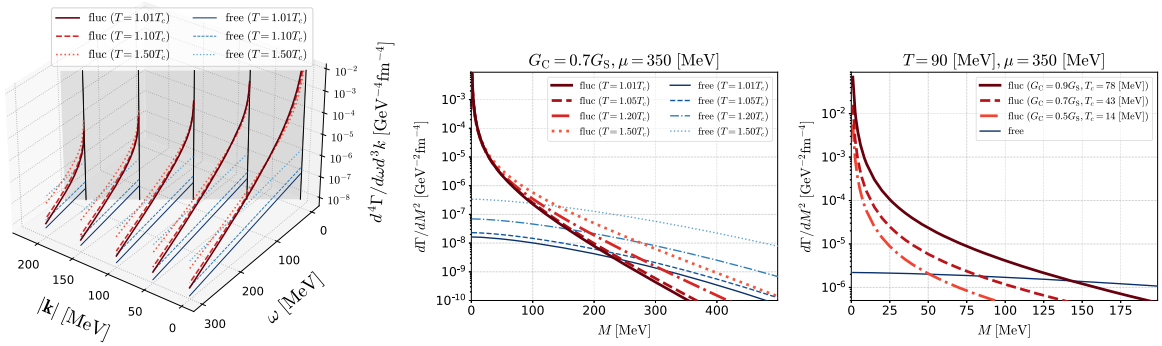

Fig. 8. Left: Dilepton production rates $d^4\Gamma/d\omega d^3k$ as a function of ω and $|\boldsymbol{k}|$ for $\mu = 350$ MeV and $T = 1.01\ T_c$, $1.1\ T_c$, and $1.5\ T_c$ at $G_C = 0.7G_S$. The gray surface shows the light cone. Middle: The invariant-mass spectrum $d\Gamma/dM^2$ for several values of T/T_c at $G_C = 0.7G_S$ and $\mu = 350$ MeV. Right: The invariant-mass spectrum $d\Gamma/dM^2$ at $(T, \mu) = (90, 350)$ MeV for $G_C = 0.9G_S$ (solid), $0.7G_S$ (dashed), and $0.5G_S$ (dash–dotted).

the small energies ω_1 and ω_2 of diquarks. The sharp peak of $d^4\Gamma/d^4k$ in Fig. 6 is understood in this way.

For more detailed properties of the enhancement of DPR, we show in the far left panel of Fig. 8 a 3D plot of DPR in the ω–$|\boldsymbol{k}|$ plane for several values of T at $\mu = 350$ MeV and $G_C = 0.7G_S$. We see that the DPR is enhanced strongly around the origin in the ω–$|\boldsymbol{k}|$ plane, and the larger the ω and/or $|\boldsymbol{k}|$, the smaller the DPR. This behavior is in accordance with the mechanism explained above.

In HIC experiments, the dilepton production rate is usually measured as a function of the invariant mass, M:

$$\frac{d\Gamma}{dM^2} = \int d^3k \frac{1}{2\omega} \frac{d^4\Gamma}{d^4k}\bigg|_{\omega=\sqrt{k^2+M^2}}. \tag{29}$$

In the middle panel of Fig. 8, we show Eq. (29) for several values of T/T_c at $G_C = 0.7G_S$ and $\mu = 350$ MeV. One sees that the enhancement due to diquark fluctuations is observed in the low-invariant-mass region $M <$ (150–200) MeV up to $T \simeq 1.5T_c$. The small T dependence of DPR seen in the very low region of M may be understood as a result of accidental cancellation between the enhanced spectral function due to the soft mode and the kinematical thermal effect: The sharp enhancement of the former at low energy–momentum near T_c decreases while the creation probability due to the thermal effect increases as T goes high. The contribution of the diquark fluctuations is relatively suppressed for higher T as the contribution of free quarks becomes larger.

Finally, shown in the right panel of Fig. 8 is $d\Gamma/dM^2$ at fixed $(T, \mu) = (90, 350)$ MeV (the cross symbol in Fig. 1) for several values of G_C. The panel shows that the production rate is more enhanced for larger G_C and T_c. For $G_C = 0.9G_S$ ($T_c \simeq 78$ MeV), the production rate from the diquark fluctuations exceeds that of the free quarks for $M \lesssim 100$ MeV.

6. Discussions

In this paper, we have investigated the effect of diquark fluctuations on the DPR near but above the critical temperature T_c of 2SC. The contribution of the diquark fluctuations was taken into account through the AL, MT, and DOS terms in the photon self-energy. We have found that the DPR is strongly enhanced in comparison with the free-quark gases in the low-energy and low-invariant-mass regions near T_c up to $T \simeq 1.5T_c$, reflecting the formation of the diquark soft mode associated with the phase transition to 2SC.

We would say that it should be rewarding to try to make an experimental measurement of dileptons in that very low-mass region and examine the possible enhancement of the DPR in HIC; if the enhancement is confirmed, it may possibly give experimental evidence of strong diquark correlations, which lead to the phase transition to 2SC in dense quark matter. We note that similar enhancement is also expected around the critical temperature of other CSC phases, such as the CFL phase, as long as the order of the phase transition is second order or weak first order. Such a measurement will be an interesting target of HIC experiments at future experimental facilities [7] that will investigate the dense medium using high-luminosity heavy-ion beams. Moreover, it is to be noted that the DPR with vanishing energy/momentum is directly related to the electric conductivity, as is evident from the fact that the AL, MT, and DOS terms in condensed matter physics are responsible for the anomalous enhancement of the electric conductivity (paraconductivity) in metals above T_c but in the close vicinity of the superconducting phase.

There are, however, many issues to be resolved for making the measurements meaningful, in the sense that it can help in revealing the significance of the diquark fluctuations prior to the phase transition to 2SC in dense matter. Since the observed yield of dileptons in HIC is a superposition of those with various origins in space-time history, we need to 'disentangle' the observed total yield into those with the respective origins. For that, it is necessary to quantitatively estimate the residence time around the phase boundary of CSC, say, with resort to dynamical models [41]. Next, although we compared the enhancement of the DPR due to the diquark soft modes with that from free-quark gases, it is known that the enhancement in the low-M region occurs in hadronic scenarios [42] and the perturbative calculation of QCD [43–45]. A comparison with these analyses is necessary to see the relative magnitudes of different production mechanisms. An analysis of the DPR under the same thermal conditions as in these approaches for the comparison constitutes important future projects. Although we confined ourselves to the dynamics in the scalar and diquark channels as seen in Eq. (1), vector coupling is known to play a significant role in determining the phase structure with CSC [5]. Thus, it would be intriguing to incorporate the vector coupling and see possible modifications of the properties of the soft modes of CSC and the DPR.

Although we discussed the enhancement of the DPR due to diquark fluctuations in the present study, as mentioned in Sect. 4 a similar enhancement can occur induced by the softening of the mesonic modes at the QCD critical point with a similar mechanism. It would be

intriguing to calculate the DPR around the critical point incorporating this effect and compare it with the result in the present study. Indeed, such an analysis is in progress and will be reported elsewhere (T. Nishimura et al., manuscript in preparation).

The experimental measurement of the DPR in the relevant low-invariant-mass region $M \lesssim 200$ MeV is not an easy task because di-electrons, which are, among dileptons, only available in this energy range, are severely contaminated by Dalitz decays, and high-precision measurements both of $d\Gamma/dM^2$ and the hadron spectrum are necessary to extract interesting medium effects. Despite these challenging requirements, it is encouraging that the future HIC programs in GSI-FAIR, NICA-MPD, and J-PARC-HI are designed to carry out high-precision experiments [7], and also that new technical developments are vigorously being made [46].

Finally, we remark that such an effort to reveal the significance of the enhanced diquark correlations in hot and dense matter should also give some clue to the modern development of hadron physics, where possible diquark correlations in hadron structures are one of the hot topics [47].

Acknowledgements

The authors thank Naoki Yamamoto for his critical comments. T.N. thanks JST SPRING (Grant No. JPMJSP2138) and the Multidisciplinary PhD Program for Pioneering Quantum Beam Application. This work was supported by JSPS KAKENHI (Grants No. JP19K03872, No. JP19H05598, and No. JP20H01903).

Funding

Open Access funding: SCOAP^3.

References

[1] K. Fukushima and T. Hatsuda, Rep. Prog. Phys. **74**, 014001 (2011) [arXiv:1005.4814 [hep-ph]] [Search INSPIRE].
[2] K. Fukushima and C. Sasaki, Prog. Part. Nucl. Phys. **72**, 99 (2013) [arXiv:1301.6377 [hep-ph]] [Search INSPIRE].
[3] M. Asakawa and K. Yazaki, Nucl. Phys. A **504**, 668 (1989).
[4] A. Barducci, R. Casalbuoni, S. De Curtis, R. Gatto, and G. Pettini, Phys. Lett. B **231**, 463 (1989).
[5] M. Kitazawa, T. Koide, T. Kunihiro, and Y. Nemoto, Prog. Theor. Phys. 108, 929 (2002); **110**, 185 (2003) [erratum] [arXiv:hep-ph/0207255] [Search INSPIRE].
[6] M. A. Stephanov, K. Rajagopal, and E. V. Shuryak, Phys. Rev. D **60**, 114028 (1999) [arXiv:hep-ph/9903292] [Search INSPIRE].
[7] T. Galatyuk, Nucl. Phys. A **982**, 163 (2019).
[8] T. Kojo, D. Hou, J. Okafor, and H. Togashi, Phys. Rev. D **104**, 063036 (2021) [arXiv:2012.01650 [astro-ph.HE]] [Search INSPIRE].
[9] M. Cierniak and D. Blaschke, Astron. Nachr. **342**, 819 (2021) [arXiv:2106.06986 [nucl-th]] [Search INSPIRE].
[10] T. Kojo, G. Baym, and T. Hatsuda; arXiv:2111.11919 [astro-ph.HE] [Search INSPIRE].
[11] M. G. Alford, A. Schmitt, K. Rajagopal, and T. Schäfer, Rev. Mod. Phys. **80**, 1455 (2008) [arXiv:0709.4635 [hep-ph]] [Search INSPIRE].
[12] A. Ohnishi, J. Phys. Conf. Ser. **668**, 012004 (2016) [arXiv:1512.08468 [nucl-th]] [Search INSPIRE].
[13] M. Kitazawa, T. Koide, T. Kunihiro, and Y. Nemoto, Phys. Rev. D **65**, 091504 (2002) [arXiv:nucl-th 0111022] [Search INSPIRE].
[14] M. Kitazawa, T. Koide, T. Kunihiro, and Y. Nemoto, Phys. Rev. D **70**, 056003 (2004) [arXiv:hep-ph/0309026] [Search INSPIRE].
[15] M. Kitazawa, T. Koide, T. Kunihiro, and Y. Nemoto, Prog. Theor. Phys. **114**, 117 (2005) [arXiv:hep-ph/0502035] [Search INSPIRE].
[16] W. Skocpol and M. Tinkham, Rep. Prog. Phys. **38**, 1049 (1975).

[17] M. Tinkham, Introduction to Superconductivity (Courier Corporation, 2004).
[18] A. Larkin and A. Varlamov, Fluctuation phenomena in superconductors, in Superconductivity (Springer, Berlin, 2008), p. 369.
[19] H. Abuki, T. Hatsuda, and K. Itakura, Phys. Rev. D **65**, 074014 (2002) [arXiv:hep-ph/0109013] [Search INSPIRE].
[20] D. N. Voskresensky, Phys. Rev. C **69**,065209 (2004) [arXiv:nucl-th/0306077] [Search INSPIRE].
[21] T. Kunihiro, M. Kitazawa, and Y. Nemoto, PoS **CPOD07**, 041 (2007) [arXiv:0711.4429 [hep-ph]] [Search INSPIRE].
[22] B. O. Kerbikov and M. A. Andreichikov, Phys. Rev. D **91**, 074010 (2015) [arXiv:1410.3413 [hep-ph]] [Search INSPIRE].
[23] B. O. Kerbikov, Phys. Rev. D **102**, 096022 (2020) [arXiv:2001.11766 [hep-ph]] [Search INSPIRE].
[24] P. Jaikumar, R. Rapp, and I. Zahed, Phys. Rev. C **65**, 055205 (2002) [arXiv:hep-ph0112308] [Search INSPIRE].
[25] L. D. McLerran and T. Toimela, Phys. Rev. D **31**, 545 (1985).
[26] H. A. Weldon, Phys. Rev. D **42**, 2384 (1990).
[27] J. I. Kapusta, P. Lichard, and D. Seibert, Phys. Rev. D **44**, 2774 (1991); 47, 4171 (1993) [erratum].
[28] T. Hatsuda and T. Kunihiro, Phys. Rep. **247**, 221 (1994) [arXiv:hep-ph/9401310] [Search INSPIRE].
[29] M. Buballa, Phys. Rep. **407**, 205 (2005) [arXiv:hep-ph/0402234] [Search INSPIRE].
[30] T. Matsuura, K. Iida, T. Hatsuda, and G. Baym, Phys. Rev. D **69**, 074012 (2004) [arXiv:hep-ph/0312042] [Search INSPIRE].
[31] I. Giannakis, D.-F. Hou, H.-C. Ren, and D. H. Rischke, Phys. Rev. Lett. **93**, 232301 (2004) [arXiv:hep-ph/0406031] [Search INSPIRE].
[32] J. L. Noronha, H.-C. Ren, I. Giannakis, D. Hou, and D. H. Rischke, Phys. Rev. D **73**, 094009 (2006) [arXiv:hep-ph/0602218] [Search INSPIRE].
[33] G. Fejős and N. Yamamoto, J. High Energy Phys. **1912**, 069 (2019) [arXiv:1908.03535 [hep-ph]] [Search INSPIRE].
[34] D. J. Thouless, Ann. Phys. **10**, 553 (1960).
[35] M. Cyrot, Rep. Prog. Phys. **36**, 103 (1973).
[36] L. Aslamazov and A. Larkin, Sov. Solid State **10**, 875 (1968) [Phys. Lett. A **26**, 238 (1968)].
[37] K. Maki, Prog. Theor. Phys. **40**, 193 (1968).
[38] R. S. Thompson, Phys. Rev. B **1**, 327 (1970).
[39] J. I. Kapusta and C. Gale, Finite-Temperature Field Theory: Principles and Applications (Cambridge University Press, Cambridge, UK, 2011), Cambridge Monographs on Mathematical Physics.
[40] M. L. Bellac, Thermal Field Theory (Cambridge University Press, Cambridge, UK, 2011), Cambridge Monographs on Mathematical Physics.
[41] Y. Nara and A. Ohnishi, Phys. Rev. C **105**, (2022) 014911. [arXiv:2109.07594] [nucl-th] [Search INSPIRE].
[42] R. Rapp, J. Wambach, and H. van Hees, The Chiral Restoration Transition of QCD and Low Mass Dileptons, Landolt-Bornstein **23** (2010) 134. [arXiv:0901.3289 [hep-ph]] [Search INSPIRE].
[43] E. Braaten, R. D. Pisarski, and T.-C. Yuan, Phys. Rev. Lett. **64**, 2242 (1990).
[44] M. Laine, J. High Energy Phys. **1311**, 120 (2013) [arXiv:1310.0164 [hep-ph]] [Search INSPIRE].
[45] J. Ghiglieri and G. D. Moore, J. High Energy Phys. **1412**, 029 (2014) [arXiv:1410.4203 [hep-ph]] [Search INSPIRE].
[46] D. Adamová et al., arXiv:1902.01211 [physics.ins-det] [Search INSPIRE].
[47] M. Y. Barabanov et al., Prog. Part. Nucl. Phys. **116**, 103835 (2021) [arXiv:2008.07630 [hep-ph]] [Search INSPIRE].